Published in final edited form as:

Immunity. 2008 August 15; 29(2): 238–248. doi:10.1016/j.immuni.2008.05.017.

A Synaptic Basis for Paracrine Interleukin-2 Signaling during homotypic T cell interaction

Catherine A. Sabatos[1,*], **Junsang Doh**[1,2,*], **Sumone Chakravarti**[1], **Rachel S. Friedman**[1], **Priya G. Pandurangi**[1], **Aaron J. Tooley**[1], and **Matthew F. Krummel**[1]

[1] Department of Pathology, University of California, San Francisco, CA 94143-0511, USA

[2] School of Interdisciplinary Bioscience and Bioengineering and Department of Mechanical Engineering, Pohang University of Science and Technology, Hyoja-Dong, Nam-Gu, Pohang, Gyeongbuk, Korea

Summary

T cells slow their motility, increase adherence and arrest after encounters with antigen-presenting cells (APCs) bearing peptide-MHC complexes. Here, we analyzed the cell-cell communication among activating T cells. In vivo and in vitro, activating T cells associate in large clusters that collectively persist for >30 minutes, but they also engaged in more transient interactions, apparently distal to APCs. Homotypic aggregation was driven by LFA-1 integrin interactions. Ultrastructural analysis revealed that cell-cell contacts between activating T cells were organized as multifocal synapses, and T cells oriented both the microtubule organizing complex and interleukin-2 (IL-2) secretion toward this synapse. T cells engaged in homotypic interactions more effectively captured IL-2 relative to free cells. T cells receiving paracrine synaptic IL-2 polarized their IL-2 signaling subunits into the synaptic region and more efficiently phosphorylated the transcription factor STAT5, likely through a synapse-associated signaling complex. Thus, synapse-mediated cytokine delivery accelerates responses in activating T cells.

Introduction

The stages of T cell trafficking, activation and arrest have been described in vivo for both $CD8^+$ (Bousso and Robey, 2003; Mempel et al., 2004) and $CD4^+$ (Miller et al., 2002; Miller et al., 2003; Miller et al., 2004) T cells. T cells initially scan dendritic cells (DCs), 'searching' for cognate peptide (Lindquist et al., 2004; Shakhar et al., 2005), and

Correspondence should be addressed to Matthew F. Krummel, HSW-512, Box 0511, 513 Parnassus Avenue, San Francisco, CA 94143-0511, Phone: 415-514-3130; FAX: 415-514-3165; matthew.krummel@ucsf.edu.

*Indicates Equal Contribution

Author Contributions

CAS performed TPLSM imaging; immunocytochemistry experiments for LFA-1, CD25, pericentrin, p-STAT5 and IL-2 and data analysis; and participated in experimental design and manuscript writing. JD performed TPLSM imaging; electron microscopy; immunocytochemistry experiments for p-STAT5, and intracellular and capture IL2 stains; LFA KO cluster experiments and analysis; and participated in experimental design and manuscript writing. SC performed clustering experiments and immunocytochemistry for LFA-1 and CD25, and participated in experimental design and data analysis. RSF performed the TPLSM for non-immunized mice and assisted in manuscript writing. PGP provided technical assistance for immunocytochemistry. AJT established the initial TPLSM work and provided technical assistance. MFK established the initial scientific questions, provided continuing intellectual guidance and participated in experimental design, analysis and manuscript writing, as well as TPLSM imaging.

The authors declare that they have no competing financial interests.

subsequently swarm and arrest on DCs (Hugues et al., 2004). The end of this phase coincides with upregulation of CD25 and the initiation of IL-2 secretion from T cells (Mempel et al., 2004). Chemokine secretion, such as CCL3 and CCL4 produced by activated DCs and T cells, increases the likelihood that T cells will co-mingle in regions where other T cells are currently, or have previously been, localized (Castellino et al., 2006; Hugues et al., 2007). This results in both long-lived and dynamic 'clusters' of T cells, responding to immunization (Bousso and Robey, 2003) or autoantigens (Tang et al., 2006). In a third phase, T cells are released from DCs, migrate once again and subsequently proliferate and gain effector function.

In vitro, the initiating cell-cell contact between a T cell and an APC has been characterized as an immunological synapse (IS) (Grakoui et al., 1999; Monks et al., 1998). Within this contact, clusters of adhesive LFA-1 molecules surround central clusters of T cell receptors (TCRs) (Grakoui et al., 1999; Monks et al., 1998). This stable contact facilitates prolonged signaling as well as polarization of surface proteins (Huppa et al., 2003; Krummel et al., 2000), the cytoskeleton (Bunnell et al., 2002; Kupfer et al., 1983) and secretory machinery (Huse et al., 2006; Stinchcombe et al., 2006) toward the APC.

Despite extensive characterization of the dynamics and nature of T cell activation, the complete impact of arrest and the ensuing changes in both T cell motility and adherence are not well elucidated. As T cells clustering upon activation has been a hallmark of activated cells both in vivo (Hommel and Kyewski, 2003; Ingulli et al., 1997) and in vitro (Inaba et al., 1984), we reasoned that motility arrest and localized aggregation of T cells might also encourage direct cell-to-cell crosstalk amongst adjacent activating T cells. We thus sought to characterize the nature of T-T cell surface interactions and the underlying cell biology within T-T clusters.

Here, we present evidence that T-T clusters promoted synaptic-based cytokine delivery between activating T cells. LFA-1 mediated multifocal synapses promoted the polarization of microtubule organizing centers and directed cytokine secretion towards adjacent T cells. These interactions are functionally important as they facilitate synapse-localized signaling complexes and activation of STAT5, a transcription factor downstream of IL-2R signaling.

Results

Prolonged cell-cell contacts between activated T cells in vivo

To gain greater insight into the dynamic nature of T cell clustering, we immunized mice with peptide in adjuvant and imaged excised lymph nodes (LNs) to specifically analyze T-T dynamics during swarming and arrest. We adoptively transferred CFSE labeled DO11.10 $CD4^+$ T cells into wild-type (WT) BALB/c recipients and activated the cells by subcutaneous (s.c.) immunization 24h later with OVA 323-339 (OVA 323) emulsified in complete Freund's adjuvant (CFA). As a control for immunization effects, we also analyzed LN draining an equivalent volume of phosphate buffered saline (PBS) and CFA. After 24h, popliteal draining (OVA-CFA) and non-draining (PBS-CFA) LN were excised, mounted to coverslips and imaged by two-photon laser scanning microscopy (TPLSM). In Figure 1, we have shown the CFSE on a pseudocolor scale where the center of the T cell body appears

red and the fainter outer region of the cell (typically dimmer because the CFSE is fainter at or just beyond the pixels bearing membrane) is color coded green. This display highlights close-associations; the green border is lost at points where the cell bodies become closely apposed (see Figure 1A-C). We found large (>3 cells, often much larger) clusters of T cells deep within the LN (>150 μm below the capsule) with persistent interactions in the draining LN (**Figure 1A**, red arrows) that remained occupied by T cells for a full 30 minutes (**Movie S1**). The frequency of the very large clusters was variable but over >5 experiments scored, we found an average of 6.6 per mm^3 of the large clusters shown in Figure 1A per LN surveyed, 18-22h after immunization. Though persistent on the whole, these large clusters were also somewhat dynamic, with ongoing evidence of coalescence, for example when multiple clusters joined (**Figure 1B**) or individual cells dissociated (**Figure 1C; Movie S2**) from existing clusters. Notably, unactivated (antigen non-specific) cells did not participate in these clusters to the same degree as activated cells (**Movie S3**).

The ability of T cells to self-associate for longer times was not purely confined to these large clusters. We also observed transient contacts that occurred when individual or small numbers of motile T cells in this phase encountered one another in regions that were otherwise devoid of our labeled cells (**Figure 1A**, white and yellow arrows). A time average of the entire field demonstrated the local persistence of cells over time at the large clusters whereas another population of smaller clusters were frequently more transient (**Figure 1A**, right panel).

For these smaller, more transient aggregates, we measured the length of time that a given T cell remained in close-association with another T cell, starting from the point at which we could first see them in close proximity. All the T-T interactions measured in control mice that received labeled cells transferred without immunization (LN taken 24h post-transfer) were 2.5 min or less in duration (mean 1.0 min), revealing a background of only short T-T interactions (**Figure 1D**). Immunization in adjuvant led to a population of intermediate length (3-6.5 min) interactions for both PBS-CFA (14.3%) and OVA-CFA (9.7%), suggesting that inflammation alone and the ensuing shift towards lower motility (Hugues et al., 2004; Shakhar et al., 2005) favors somewhat longer interactions. Relative to this non-specific background, peptide-specific immunization (OVA-CFA) gave rise to a population (9.2% of all T-T encounters) with longer-kinetics (**Figure 1D**). Although this population was not large and the maximal duration of these transient T-T clusters rarely exceeded 10 minutes, if extended over many hours, accumulated small T-T cluters are likely to result in additional associations for cells during the course of activation.

APC-dependent or independent stimuli result in dynamic LFA-1 mediated T cell cluster assembly in vitro

While TPSLM is ideally suited to studying the dynamics of cell-cell association, an in vitro system was required to ascertain the exact nature of the cell-cell contact. By engaging TCRs on T cells in vitro in the presence or absence of APCs, we studied the requirement for APCs in mediating T cell homotypic adhesion.

Whole LN preparations from DO11.10 mice were activated with titrated doses of OVA peptide, and cluster size was tracked over 72h. As with the in vivo setting, activation-

induced T-T aggregation began approximately 16h after stimulation, and cells joined over time to form larger arrays of T cells in clusters. Clustering kinetics and extent was antigen dose-dependent (**Figure 2A**). Furthermore, self-aggregation by T cells stimulated with either CD3 antibody plus CD28 antibody or phorbol 12-myristate 13-acetate (PMA) plus ionomycin in the absence of APCs indicated that this ability to self-aggregate is a capacity gained after cell activation but not absolutely requiring a nucleating APC (**Figure 2B**).

Clusters generated in the absence of APC-based immunological synapses also resembled the in vivo scenario insofar as the T cells in the clusters remained motile and associations were highly dynamic. As shown in **Figure 2C** and **Movie S4**, we seeded 10% CFSE-labeled $CD4^+$ C57BL/6 T cells into a culture with identical unlabeled cells and activated for 18h with PMA and ionomycin. The resulting clusters demonstrated both stability (yellow arrow) and plasticity, with T cells both joining (red arrow) and leaving (white arrow) clusters similarly to that seen in vivo. The ongoing cell motility in vitro and high plasticity argues against a random aggregation model and instead suggests that T cells actively engage in stable interactions with one another in the course of ongoing motility and might do so via specific mechanisms, such as integrin-mediated adhesion.

Given that the primary T cell integrin, LFA-1, is required for initiation of activation when APCs are stimulators, we used APC-independent activating stimuli to probe the role of LFA-1 in driving self-aggregation of $CD4^+$ T cells. This permitted study of T cells derived from LFA-1-deficient (*Itgb2*$^{-/-}$) mice or for WT cells in the presence of blocking antibody against LFA-1 (anti-CD11α). There was a significant reduction (two-sample $t(93)=1.986$, $p=1.75\times10^{-12}$)of activation-induced T cell clustering in cells from *Itgb2*$^{-/-}$mice (**Figure 2D, E**) activated with PMA and ionomycin, as compared to cells from wild-type mice. After cluster assembly, and in accord with previous studies (Rothlein and Springer, 1986) the addition of CD11α antibody, but not antibodies against other adhesion receptors (including Jam-1, MAC-1, VCAM, α4, and α4β7; data not shown), effectively dispersed these aggregates in WT $CD4^+$ T cells (two-sample $t(94)=1.986$, $p=1.14\times10^{-13}$), demonstrating that LFA-1 serves as a primary source of adhesion for T-T contacts (**Figure 2D,E**). Similar results were observed using anti-CD3 plus anti-CD28 stimulation (data not shown). This confirmed that T-T clustering in vitro is activation-mediated, but does not require a bridging DC. Staining of clusters with antibodies to LFA-1 (**Figure S1**) also showed specific enrichment of this protein in the regions of close juxtaposition, further highlighting that this process is active rather than passive. Notably, only modest enrichment of CD86 (**Figure S1**), MHC, TCR, CD4 and CD28 (not shown) were observed in T-T synapses which contrasts these with the IS formed between T cells and APCs (Krummel et al., 2000; Monks et al., 1998; Pentcheva-Hoang et al., 2004).

T-T Interactions Proximal and Distal to T-APC synapses

T-T interactions are activation-induced, as evidenced by the requirement both in vitro and in vivo for TCR stimulation preceding T-T clustering (Figures 1-2). The data in Figure 2 suggested that DCs are not required to mediate homotypic aggregation. However, to determine the relative DC-dependence or independence of T-T interactions when stimulation is driven by DCs in vivo or in vitro, we localized DCs within the context of

clusters. To achieve this in vivo, we transferred CMTMR-labeled OT-II $CD4^+$ T cells into CD11c-YFP mice (Lindquist et al., 2004), immunized subcutaneously with OVA-CFA, and imaged draining LN via TPSLM after 24h. As shown in **Figure 3A** and **Movie S5**, the vast majority of T cells form large clusters around DCs, with T cells concurrently engaging in homotypic interactions. We also were able to visualize the smaller cohort of T cells engaging in homotypic interaction at some distance from the nearest DC (**Figure 3A**). It is worth noting that very thin dendrites may project from the DC in Figure 3A and so it is not formally possible in this context to exclude a role for DCs in the aggregate. Additionally, given the density of DCs within the T cell zone of the LN, DCs are certainly always very nearby.

Similarly, T-T interactions proximal to and distal from the DC body were observed in vitro when OT-II $CD4^+$ T cells were activated by CFSE-labeled Bone-marrow derived dendritc cells (BMDC), pre-pulsed with OVA 323. As shown in **Figure 3B**, T cells tightly packed around central DCs (blue), and additional T cells extended to peripheral parts of the cluster, away from close contact with the nucleating DC. Again, although small dendrites may assist in these contacts, taken together with the data from Figure 2, it appears likely that activating T cells acquire some affinity for one another, independent of DCs.

T-T Contacts are Mediated by Multifocal Synapses

The T-T cluster requirement for adhesion molecules and formation in the absence of added or apparent APCs both in vivo and in vitro suggested that a homotypic LFA-1 mediated synapse-like structure might facilitate T-T interactions in a similar fashion to T cell-APC synapses. Electron microscopy (EM) analysis demonstrated that T-T synapses formed between activated T cells with strong membrane apposition similar to that seen at a typical IS between a T cell and DC (Brossard et al., 2005) (**Figure 4A**). Of particular note are the synaptic spaces (arrows in **Figure 4B**) at the contacts, indicative of a multifocal synapse with substantial intercellular volume enclosed by the apposed membranes. Furthermore, EM sections in which intracellular vesicles could be observed frequently showed those vesicles to be oriented toward the adjacent T cells (**Figure 4C**), further suggesting that these encounters were not passive.

Polarized MTOC and secretion of IL-2 at T-T Synapses

Reorientation of a migrating cell upon pMHC-induced arrest results in the polarization of the Golgi apparatus and MTOC toward the point of contact, allowing for the alignment of intracellular organelles and secretion of effectors into the synapse (Kupfer et al., 1983). Staining for the MTOC-associated protein pericentrin at T-T synapses (**Figure 5A**) indicated an 80% bias in the polarization of the tubulin cytoskeleton inward toward adjacent T cells. In **Figure 5A**, right panel, we assessed whether this bias was due to specific polarization of pericentrin as opposed to simple availability of T-T contact interface versus free membrane. If the bias toward polarization ‘in’ were due simply to a high percentage of available T-T contact interface (versus free membrane), one would predict that the percent of T-T contact would correlate directly to the percentage of protein facing inward (i.e., 10% T-T contact and 90% free membrane results in 10% pericentrin ‘in’ and 90% pericentrin ‘out’). However when tested against this hypothesis, the observed percentage of pericentrin facing ‘in’ was

significantly higher than that predicted for 0-33% (p=0.00001) and 33-66% (p=0.002) T-T contact (**Figure 5A**, graph). This suggested that activating T cells selectively polarize toward one another, potentially to facilitate the organization of effector molecules, secretion and signaling at T-T interfaces. To directly test whether T-T synapses polarized cytokine secretion, we stained aggregates for intracellular IL-2. As previously demonstrated (Huse et al., 2006), IL-2 containing vesicles were directionally polarized toward APCs when an APC is the neighboring cell (**Figure 5B**, small arrow). However, when T cells on the edge of large aggregates (only including those where molecules had the 'choice' of inward or outward polarization) were examined for the polarization of intracellular IL-2, there was a strong bias (84.6%) of these vesicles toward polarization to an adjacent T cell (**Figure 5B**, large arrows). Similarly, when large aggregates of T cells, activated independently of APC by PMA plus ionomycin, were examined, over 80% of all contacts demonstrated strong polarization of IL-2 pools facing inwards (**Figure 5C** and associated graph).

T-T Synapses Facilitate Capture of Secreted Cytokines

The data from Figure 5 strongly suggested that T cells in clusters would have a benefit in terms of their exposure to IL-2 as a result of the localized secretion. To test whether this is the case, we took advantage of a 'catch' antibody-detection system which uses a surface-binding antibody to locally capture IL-2 on the cell that is exposed to it. By coating cells with this antibody prior to activating them with an APC-independent stimulus (**Figure 6A**, left), we were able to reveal accumulated IL-2 in clusters, to determine whether T cells in these arrays were preferentially exposed to IL-2 relative to those that did not participate. This assay revealed that T cells in clusters (**Figure 6B**) accumulated puncta of IL-2 on their surface and that this surface accumulation was almost universally directed inward toward the cluster (isolated 2-cell cluster shown in **Figure 6C; Movie 6** for 3D rendering). In contrast, cells from the same culture condition that were not involved in a cluster (**Figure 6D**) had two-fold less fluorescence intensity per cell on average, a measure of the total amount of IL-2 captured (**Figure 6E**). The staining pattern for these was typically much more even, although faint puncta on the surface could occasionally be discerned; perhaps a result of a synaptic delivery during a transient encounter. To rule out the possibility of aggregation of the 'catch' antibody itself in the synaptic space, we also coated cells with catch reagent after stimulation and fixing, and stained with rhodamine conjugated secondary antibody against catch reagent (**Figure 6A**, right). The bright puncta were not evident in clusters (**Figure 6F**) and the intensity of clustered and free cells for this marker was indistinguishable (**Figure 6G**). This supports the interpretation that IL-2 was locally captured on the catch reagents in Figure 6B and subsequently detected as T-T localized puncta. Furthermore, the data support the point that cells that are not engaged in synaptic contacts accumulate less synaptic IL-2 (indeed, also less overall [**Figure 6E**]) as compared to synapse-engaged T cells.

IL-2 signaling is Polarized at T-T Synapses

The data above suggested a synaptic basis for IL-2 signaling between activated T cells. IL-2 binds to a non-signaling alpha chain (CD25) as well as two signaling-competent beta and gamma chains (CD122 and CD132 (γc), respectively). Although antibodies against CD122

were not sensitive enough for staining, we found that both CD25 and CD132 were accumulated in the T-T interfaces, although the former in particular was not always uniformly expressed at high amounts as it is upregulated to varying extent in individual T cells over activation. Assessment of accumulation of surface proteins is difficult for multicellular clusters when all the cells in the clusters express the receptor and is also subject to artefacts due to a local increase of total membrane in the synaptic region (typically more than two cells contribute membrane to the same detection space). To control for this factor, we co-stained cells with lipophilic DiIC, a far-red dye that intercalates into membranes and thus is a surrogate marker for local membrane density. We demonstrated that regions of T-T synapses were also enriched in DiIC staining **(Figure 7A)**. By comparing the normalized cell surface staining intensities along the surface to DiIC staining, we demonstrated that CD25 enrichment typically was no greater in the synaptic region (highlighted by arrows) as compared to total membrane accumulation (**Figure 7B**) and may in fact be more highly represented outside of the contact region. In contrast, CD132, the signaling subunit, showed strong accumulation in the synaptic region, even when compared to the total membrane. This accumulation typically corresponded to a prominent dot, which was evident in the contacts as visualized with CD132 or in the CD132-DiIC overlay.

IL-2 signaling through CD122 and the common gamma chain (CD132; γc) triggers association of STAT5 with the membrane and coordinates its subsequent phosphorylation by Jak kinase family members (Lin and Leonard, 2000). When aggregated T-T clusters were stained for the phosphorylated form of STAT5 (p-STAT5), substantially greater p-STAT5 accumulated within clustered T cells than in ‘free’ cells found outside the confines of a cluster (**Figure 7C, D**). In contrast to free T cells, the mean fluorescence intensity (MFI) of p-STAT5 did not adhere to a normal distribution; rather, 37% of clustered cells were markedly brighter for p-STAT5 than the brightest free cell (**Figure 7D**).

In addition, the vast majority of clustered T cells examined showed p-STAT5 puncta facing inward toward other T cells, strongly suggesting a local activation of this molecule at the site of T-T contacts (**Figure 7E, F**). Some of these puncta also faced T-DC contacts consistent with localized stimulation of γc cytokine receptors at these synapses. Similarly to that seen with pericentrin (**Figure 5A**), p-STAT5 polarization was specific, irrespective of the available amount of T-T versus free membrane surface (**Figure 7F**). p-STAT5 and IL-2 were polarized in the same direction at T-T interfaces in 75% of interfaces analyzed (in 31 counted clusters) (**Figure 7G**). This polarization of p-STAT5 and IL-2 toward one another on facing T cells is similar to the mutual exclusion of IL-2 production and STAT5 activation observed by flow cytometry in previous studies (Long and Adler, 2006) and emphasizes the importance of paracrine IL-2 signaling in facilitating T cell activation. Thus, T-T synapses facilitate synapse-based IL-2 signaling, consistent with polarized secretion from the cells across the synapse.

Discussion

T-T clusters have long been considered a correlate of efficient T cell activation. Here, we supply new evidence that activated T cell clusters result in the establishment of multifocal synapses through which cytokines are directionally shared. These contacts are synapses by a

number of distinct criteria, used to compare neuronal and immunological synapses (Dustin and Colman, 2002). These include that they are dynamic but stabilized, utilize adhesive LFA-1 molecules for their formation, retain their distinct identities with a gap between their apposed membrane surfaces, and most importantly meet the functional criteria of facilitating directed secretion via polarizing the MTOC as well as signaling molecules IL-2 and p-STAT-5. We also provide evidence that these interactions are functionally important insofar as T cells that form these contacts generate stronger signals when compared to those that activate without cell-cell contact.

Interestingly, T-T association in vivo and in vitro occurs not only during stable interactions with APCs but also during 'swarming' interactions, when clusters are dynamic. Recent evidence suggests that the IS between a T cell and APC is in fact a more dynamic structure than initially recognized, with PKCtheta driven migration phases required for IL-2 production (Sims et al., 2007). Transient interactions between T cells and APCs have been described as a period for augmentation of antigenic signals (Miller et al., 2004) and may, in the case of T-T interactions, be used for enhanced IL-2 signaling and subsequent T cell activation, potentially at the onset of proliferation.

The specificity by which activated T cells cluster remains to be discovered. Our data show, as has been demonstrated previously (Rothlein and Springer, 1986; Rothlein et al., 1986; van Kooyk et al., 1989), that LFA-1 interactions between T cells are an integral part of assembly. Although the upregulation of both LFA-1 avidity and ICAM-1 expression during activation may in part mediate specificity such that already activated T cells tend to synapse (Rothlein et al., 1986), it is also possible that a unique class of activation-driven receptors that favor synaptic interactions remain to be identified. In this light, γc cytokines are not themselves required for T-T interactions (CS, JD, and MFK, data not shown).

The localized distribution of γc cytokine receptors in T cells activated in the context of a cell-cell contact also represents an expansion of the complexity of this signaling pathway. Although our data demonstrate clearly enhanced amounts of p-STAT5 in T cell clusters overall and a substantial amount of this within the nuclear region, we were surprised by the enrichment of the phosphorylated (active) form directly adjacent to the receptor. This observation in particular may indicate that the localization of activating cytokine receptors along the membrane may generate signalosomes whose molecular players are determined by a wider variety of signaling receptors than the cytokine itself. Unique localization in a synapse may thus underlie the unique outcomes of IL-2 and IL-15 signaling, both of which are generated in part through STAT5 (Lin and Leonard, 2000).

The T-T synaptic localization of cytokines and their receptors may also support the 'transpresentation' of γc cytokines on their alpha chains. Recently, it has been shown that the IL-2Rα chain in particular is critical in driving T cell help for the establishment of $CD8^+$ T cell effector functions and memory (Janssen et al., 2005; Williams et al., 2006) and that this can be mimicked by anti-IL-2-IL-2 Ab complexes (Boyman et al., 2006) when the Fc portion of IL-2 antibody was preserved. The IL-2 crystal structure revealed that binding of IL-2Rα to IL-2 may stabilize a secondary binding site for presentation to IL-2Rβ, with γc subsequently recruited by this complex (Wang et al., 2005). Similarities in the carboxyl

termini of IL-15Rα (known to transpresent IL-15) and IL-2Rα have strengthened the notion that IL-2 may also be presented in *trans* (Chirifu et al., 2007). In our data, it is notable that the accumulation of the gamma chain (CD132) was much more pronounced than for the alpha chain (CD25), perhaps suggesting that only the former is clustered whereas the latter 'catches' IL-2, perhaps relatively independently. Alternatively, the localized secretion of IL-2 seen at these tight T-T junctions may negate the need for IL-2Rα transpresentation and allow for direct IL-2-γc signaling.

Paracrine IL-2 has been shown to be sufficient for a fully functional $CD8^+$ memory T cell response in the case of a primary helpless stimulation (Williams et al., 2006), a function that could be fulfilled by $CD4^+$ T cells directing or presenting IL-2 to $CD8^+$ T cells using the mechanism we elaborated here. Chemokine-mediated attraction of naïve $CD8^+$ T cells to areas of activated $CD4^+$ T-DC interactions has been described recently (Castellino et al., 2006), and T-T interactions may facilitate the sharing of IL-2 in this context.

The data presented herein is consistent with previous reports that show IL-2 polarizes toward APCs (Huse et al., 2006), but also presents the important extension that IL-2 secretion is also specifically polarized between adjacent T cells. It is also highly consistent with flow cytometry experiments demonstrating that IL-2 producing cells were rarely enriched with p-STAT5 (Long and Adler, 2006); a result that may, in this light, be caused by synaptic interactions between IL-2 producers and those that do not produce the cytokine but rather receive the resultant signals. In the case of a number of cytokines for which receptors lie only on other T cells and not APCs, this may represent an important means of influencing the activation and differentiation of neighboring cells. In particular, T helper cell cytokine feedback may allow a collection of clones to come to a quorum decision and/or assist a pre-existing differentiated clone to influence the response of newly activating clones.

Our results here remain to be extended to known pathogenic and clonally diverse situations. It is clear that our studies utilize high precursor frequencies for a single peptide and would typically be higher than a normal naïve repertoire for pathogens. The inflammatory chemokines CCL3 and CCL4 have been shown to attract activating T cells towards one another (Castellino et al., 2006; Hugues et al., 2007) and may play a role in enhancing synaptic exchange of cytokines. Notably, though, the mechanism we describe may have greatest relevance in secondary responses or when expanded memory effector cells are activated alongside new clones. We have also recently detected clusters with similar dynamics in polyclonal T cell populations in the draining LN during secondary responses to LCMV (R. Friedman, J. Hu, M. Krummel and M. Mattloubian, data not shown). Synaptic contacts may, in this context, assist lower affinity clones or boost stimulation as antigen concentrations decrease post-infection. As such, the cell biology of T-T synapses is likely to prove important in numerous other immunological settings.

Experimental Procedures

Mice

BALB/c, C57BL/6, Actin-CFP, LFA-1-deficient *Itgb2*$^{-/-}$, DO11.10 TCR tg and OT-II TCR tg mice were purchased from The Jackson Laboratory. DO11.10 mice express a TCR

specific for chicken ovalbumin amino acids 323-339 (called 'OVA 323' here) in the context of MHC class II molecule I-A^d and were crossed with BALB/c mice to obtain heterozygous DO11.10 mice. OT-II tg mice also express an OVA peptide specific TCR that pairs with the CD4 co-receptor, in the context of MHC class II molecule I-A^b; OT-II mice were crossed with C57BL/6 mice to obtain heterozygous OT-II mice. Actin-CFP mice express a transgenic construct containing an Enhanced Cyan Fluorescent Protein gene under the control of a chicken β-actin promoter coupled with the cytomegalovirus (CMV) immediate early enhancer. CD11cYFP mice (Lindquist et al., 2004) were a kind gift of Dr. Michel Nussenzweig. All mice were bred and maintained in accordance with the guidelines of the Lab Animal Resource Center of the University of California, San Francisco.

Antibodies

Anti-LFA-1 (M17/4), fluorescein isothiocyanate-conjugated monoclonal anti-CD25 (2A3) and biotinylated anti-IL-2 (JES6-5H4) were obtained from BD Pharmingen. Biotinylated polyclonal anti-IL-15Rα was obtained from R&D Systems. Anti-phosphorylated-STAT5 (Tyr694) was obtained from Cell Signaling Technology. Polyclonal anti-pericentrin was obtained from Covance. Secondary antibodies (Jackson Immunoresearch) utilized were rhodamine-conjugated donkey-anti-rat, rhodamine-conjugated donkey-anti-goat and rhodamine-conjugated streptavidin. Anti-CD3 (500.A2) and anti-CD28 (37N51.1) antibodies were prepared from cultured hybridoma supernatant using standard Protein A/G Ab purification methods.

Immunocytochemistry

$CD4^+$ T cells were purified from spleen (SPN) and LN cells from DO11.10 and OT-II mice by negative selection using the $CD4^+$ negative selection StemSep purification kit (Stem Cell Technologies, Inc.) or MACS kit (Miltenyi Biotec), with MACS LS+ selection columns. Purified $CD4^+$ T cells (4×10^5) were activated in 96-well flat bottom plates (Fisher Scientific) for 19-20h at 37°C, 5%CO2 with 10 ng/ml phorbol 12-myristate 13-acetate (PMA; Sigma-Aldrich) and 0.5 μg/ml ionomycin (Sigma-Aldrich), or actin-CFP^+ BMDC (1×10^5) (grown in GM-CSF and IL-4; LPS-matured), pre-pulsed with OVA peptide (10 μg/ml; AnaSpec). Media used was RPMI 1640 (Gibco) supplemented with 10% fetal calf serum (JRH Biosciences), L-Glutamine (UCSF Cell Culture Facility, 2mM), Pen-Strep (Gibco, 100 units/ml and 100 μg/ml, respectively) and β-mercaptoethanol (Sigma, 50 μM) (R10 media). Staining was then performed at room temperature (RT). Briefly, cell clusters were gently harvested and fixed to poly-lysine coated Superfrost slides (VWR) with 1% paraformaldehyde (PFA; Electron Microscopy Services) for 10 min, and slides were then centrifuged to adhere the cells to the slide. Fixed cells were blocked in wash buffer with 1% FCS (and 2% normal donkey serum for slides where secondary donkey antibodies were used) and were permeabilized for 30 min with 0.02% saponin (Sigma) in PBS. Cells were incubated for 60 min with primary antibodies, washed extensively and stained with secondary antibody for 60 min. DAPI (4', 6-diamidino-2-phenylindole) was used in the final wash where indicated. Cells were then washed overnight and treated with antifade reagent (BioRad), after which slides were sealed and imaged. A modified Zeiss Axiovert 200M microscope with a plan-neofluar 40X objective (Carl Zeiss, Inc.) was used for imaging experiments. The microscope was fitted with dual excitation and emission filter wheels and

a Photometrics Coolsnap-HQ camera. The imaging and control software used was Metamorph (Universal Imaging, Molecular Devices, Corp.).

For experiments where DiIC was used to quantify membrane, cells were stained with DiIC ((DiIC 18 [1,1'-dioctadecyl-3,3,3',3'-tetramethylindocarbocyanine perchlorate]),Invitrogen) for 5 min at RT prior to fixation and staining.

To determine the percentage of total pericentrin-, IL-2- or p-STAT-5-positive T cells with pericentrin, IL-2 or p-STAT-5 facing toward or away from another T cell, only the cells in the outermost layer of a cluster (i.e., where the marker could potentially face toward or away from an adjacent cell) were counted. The marker was scored as facing toward an adjacent T cell if it was within the first third of the cell membrane juxtaposed to another T cell membrane. To determine the percentage of total IL-2- or p-STAT-5-positive T cells with IL-2 or p-STAT-5 facing toward or away from a DC, all cells were counted as in all instances the marker could potentially face toward or away from the DC. Linescans were performed in Metamorph and intensities along the line were normalized by dividing by the sum of the total intensities of all points along the membrane.

Electron Microscopy

12×10^6 Balb/c WT $CD4^+$ T cells were stimulated with PMA (5 ng/ml) and ionomycin (125 ng/ml) in 3 ml of R10 media in a 6 well plate. 18h post-stimulation, 3 ml of pre-warmed 3% glutaraldehyde/1% PFA (0.1 M cacodylate buffer, pH 7.4) was applied, and cells were fixed at 37°C for 20 min and stored at 4°C. Fixed cells were then rinsed in water, post-fixed in reduced OsO4 (2% OsO4 + 1.5% potassium ferrocyanide, Sigma, prepared fresh) and stained en bloc with uranyl acetate before being dehydrated in ethanol, cleared in propyline oxide, and embedded in eponate 12 (Ted Pella Co.). Thin sections were cut by Leica Ultracut UCT microtome, and examined under a Philips Tecnai 10 electron microscope.

Cluster analysis

Purified $CD4^+$ DO11.10 TcR tg T cells were stimulated with PMA and ionomycin as described above or with plate-bound CD3 antibody (flat bottom, 96 well plates pre-coated with 50μl/well Ab for 1h at 37°C, or overnight at 4°C, and washed extensively) in titrated concentrations from 0.1 to 1 μg/ml and soluble CD28 antibody (added at beginning of assay at 5 μg/ml). LFA-1 antibody (20 μg/ml) was added at 18h after initial stimulation, and wells were photographed at 20h. Wells were photographed at one to four spots/well (2-3 wells/condition) at noted timepoints, and cluster area was measured with Metamorph software. Where indicated BMDCs were labeled with CMAC ((7-amino-4-chloromethylcoumarin), Invitrogen).

For time-lapse microscopy of clusters, $CD4^+$ T cells were purified from C57BL/6 mice, and some of the purified T cells were labeled with CFSE. 3×10^5 T cells (90% unlabeled and 10% CFSE labeled, in R10 media with 0.1% low-melt agarose) were stimulated by PMA (5 ng/ml) and ionomycin (125 ng/ml) in 8 well Lab-Tek chamber (Nunc). Time-lapse microscopy was performed 18h after stimulation.

IL-2 Capture Assay

$CD4^+$ T cells purified from Balb/c WT mice were coated with mouse IL-2 catch reagent of mouse IL-2 secretion assay detection kit (Miltenyi Biotec) by incubating T cells in 20X dilution of IL-2 catch reagent in R10 media for 15 min in ice and washing once with R10 media. Then, the IL-2 catch reagent coated T cells were stimulated with PMA/ionomycin in a flat bottom 96 well plate for 19h. Activated T cells were transferred to 8 well Labtek chambered coverslips (Nunc) coated with poly-lysine, incubated 15 min at 37°C with 5% CO2, spun at 1500 rpm for 5 min, fixed with 1% PFA for 15 min at 4°C, and stained with PE (Phycoerythrin)-conjugated IL-2 detection antibody (1:20 dilution in R10 media). Finally, 1% low-melt agarose was added to the wells, and Labtek wells were spun at 1500 rpm at RT. Samples embedded in agarose gel were examined with a spinning disk confocal microscope (Yogogawa, Japan). Single plane bright field images and z-stack of red fluorescence images (0.4 um intervals) were acquired with 40x objective lens (Nikon, NA 1.3). Acquired images were analyzed using Metamorph. Fluorescence intensity was integrated over the volume of single cells or clustered cells after background subtraction. For clustered cells, the integrated fluorescence intensity was divided by the number of cells in the clusters to obtain integrated fluorescence intensity per cell.

Statistical Analyses

The Chi-squared test and Student's t test were utilized, as indicated in the text. All p values <0.05 were considered significant.

TPLSM acquisition

$CD4^+$ T cells purified from DO11.10 or OT-II mice as described above were labeled with carboxyfluorescein diacetate, succinimidyl ester (CFSE; Invitrogen) or with CMTMR ((5-(and-6)-[4-chloromethyl(benzoyl)amino] tetramethylrhodamine), Invitrogen) at 5μM for 10 min at RT. Cells were washed extensively, and 5×10^6 dye-labeled cells were intravenously transferred to WT BALB/c or C57Bl/6 CD11c-YFP recipients. 24h later, mice were immunized s.c. in the footpads with 25 μg OVA peptide emulsified in CFA (Sigma) or PBS-CFA as a control, or left unimmunized as a control. A further 24h later, popliteal LN were immobilized on coverslips with the hilum facing away from the objective. A custom resonant-scanning instrument (Tang et al., 2006) containing a four-photomultiplier tube operating at video rate was used for two-photon microscopy. LN were maintained at 36°C in RPMI medium bubbled with 95%O2 and 5%CO2 and were imaged through the capsule distal to the hilum. Samples were excited with a 5-W MaiTai TiSaphire laser (Spectra-Physics) tuned to a wavelength of 810 nm, and emission wavelengths of 500-540 nm (for CFSE) and 380-420 nm (for detection of second-harmonic emission) were collected. A custom four-dimensional acquisition module in VideoSavant digital video recording software (IO Industries) was utilized for image acquisition. Each LN was first surveyed in a raster scan for the presence of transferred cells. Adjacent z-stacks of up to 350 μm encompassing the top *xy* space of the lymph node were collected. For time-lapse acquisition, each *xy* plane spanned 330 μm × 230 μm at a resolution of 0.6 μm per pixel, and ten video-rate frames were averaged, giving effective collection time of approximately 330 ms per

image. Images of up to 30 *xy* planes with 5 μm *z*-spacing were acquired every 30s for 30 min. Images were analyzed with Imaris software.

Dwell time of T-T interactions was measured by tracking the length of time that a given T cell remained in close-association (<10 μm) with another T cell. The measured value does not consider additional numbers of associated cells. For example, in some images, a T cell pair joined a second T-T pair and then separated. When each pair still retained a T-T contact, this additional contact was not considered and the dwell time represents when a given T cell ceased to have any T-T association.

Supplementary Material

Refer to Web version on PubMed Central for supplementary material.

Acknowledgements

We would like to thank Fred Siedenberg and Larry Braun (Sutter Instruments) and Ivy Hsieh (electron microscopy) for technical assistance; and Averil Ma and Abul Abbas for helpful discussion. This work was supported by NIH training grant #5T32AI007334 (CAS), a National Multiple Sclerosis Society Postdoctoral Fellowship (SC), by startup funds from the HHMI Biomedical Research Support Program (grant #5300246) and by the Juvenile Diabetes Foundation (MFK).

Non-standard Abbreviations

MTOC	microtubule organizing complex
TPLSM	2 photon laser scanning microscopy
EM	electron microscopy
p-, c-SMAC	peripheral and central supramolecular activating complex
MFI	mean fluorescence intensity

References

Bousso P, Robey E. Dynamics of CD8(+) T cell priming by dendritic cells in intact lymph nodes. Nat Immunol. 2003; 4:579–585. [PubMed: 12730692]

Boyman O, Kovar M, Rubinstein MP, Surh CD, Sprent J. Selective stimulation of T cell subsets with antibody-cytokine immune complexes. Science. 2006; 311:1924–1927. [PubMed: 16484453]

Brossard C, Feuillet V, Schmitt A, Randriamampita C, Romao M, Raposo G, Trautmann A. Multifocal structure of the T cell - dendritic cell synapse. Eur J Immunol. 2005; 35:1741–1753. [PubMed: 15909310]

Bunnell SC, Hong DI, Kardon JR, Yamazaki T, McGlade CJ, Barr VA, Samelson LE. T cell receptor ligation induces the formation of dynamically regulated signaling assemblies. J Cell Biol. 2002; 158:1263–1275. [PubMed: 12356870]

Castellino F, Huang AY, Altan-Bonnet G, Stoll S, Scheinecker C, Germain RN. Chemokines enhance immunity by guiding naive CD8+ T cells to sites of CD4+ T cell-dendritic cell interaction. Nature. 2006; 440:890–895. [PubMed: 16612374]

Chirifu M, Hayashi C, Nakamura T, Toma S, Shuto T, Kai H, Yamagata Y, Davis SJ, Ikemizu S. Crystal structure of the IL-15-IL-15Ralpha complex, a cytokine-receptor unit presented in trans. Nat Immunol. 2007; 8:1001–1007. [PubMed: 17643103]

Dustin ML, Colman DR. Neural and immunological synaptic relations. Science. 2002; 298:785–789. [PubMed: 12399580]

Grakoui A, Bromley SK, Sumen C, Davis MM, Shaw AS, Allen PM, Dustin ML. The immunological synapse: A molecular machine that controls T cell activation. Science. 1999; 285:221–226. [PubMed: 10398592]

Hommel M, Kyewski B. Dynamic changes during the immune response in T cell-antigen-presenting cell clusters isolated from lymph nodes. J Exp Med. 2003; 197:269–280. [PubMed: 12566411]

Hugues S, Fetler L, Bonifaz L, Helft J, Amblard F, Amigorena S. Distinct T cell dynamics in lymph nodes during the induction of tolerance and immunity. Nat Immunol. 2004; 5:1235–1242. [PubMed: 15516925]

Hugues S, Scholer A, Boissonnas A, Nussbaum A, Combadiere C, Amigorena S, Fetler L. Dynamic imaging of chemokine-dependent CD8+ T cell help for CD8+ T cell responses. Nat Immunol. 2007; 8:921–930. [PubMed: 17660821]

Huppa JB, Gleimer M, Sumen C, Davis MM. Continuous T cell receptor signaling required for synapse maintenance and full effector potential. Nat Immunol. 2003; 4:749–755. [PubMed: 12858171]

Huse M, Lillemeier BF, Kuhns MS, Chen DS, Davis MM. T cells use two directionally distinct pathways for cytokine secretion. Nat Immunol. 2006; 7:247–255. [PubMed: 16444260]

Inaba K, Witmer MD, Steinman RM. Clustering of dendritic cells, helper T lymphocytes, and histocompatible B cells during primary antibody responses in vitro. J Exp Med. 1984; 160:858–876. [PubMed: 6206192]

Ingulli E, Mondino A, Khoruts A, Jenkins MK. In vivo detection of dendritic cell antigen presentation to CD4(+) T cells. J Exp Med. 1997; 185:2133–2141. [PubMed: 9182685]

Janssen EM, Droin NM, Lemmens EE, Pinkoski MJ, Bensinger SJ, Ehst BD, Griffith TS, Green DR, Schoenberger SP. CD4+ T-cell help controls CD8+ T-cell memory via TRAIL-mediated activation-induced cell death. Nature. 2005; 434:88–93. [PubMed: 15744305]

Krummel MF, Sjaastad MD, Wülfing C, Davis MM. Differential Assembly of CD3ζ and CD4 During T cell Activation. Science. 2000; 289:1349–1352. [PubMed: 10958781]

Kupfer A, Dennert G, Singer SJ. Polarization of the Golgi apparatus and the microtubule-organizing center within cloned natural killer cells bound to their targets. Proc Natl Acad Sci U S A. 1983; 80:7224–7228. [PubMed: 6359165]

Lin JX, Leonard WJ. The role of Stat5a and Stat5b in signaling by IL-2 family cytokines. Oncogene. 2000; 19:2566–2576. [PubMed: 10851055]

Lindquist RL, Shakhar G, Dudziak D, Wardemann H, Eisenreich T, Dustin ML, Nussenzweig MC. Visualizing dendritic cell networks in vivo. Nat Immunol. 2004; 5:1243–1250. [PubMed: 15543150]

Long M, Adler AJ. Cutting edge: Paracrine, but not autocrine, IL-2 signaling is sustained during early antiviral CD4 T cell response. J Immunol. 2006; 177:4257–4261. [PubMed: 16982857]

Mempel TR, Henrickson SE, von Andrian UH. T-cell priming by dendritic cells in lymph nodes occurs in three distinct phases. Nature. 2004; 427:154–159. [PubMed: 14712275]

Miller MJ, Safrina O, Parker I, Cahalan MD. Imaging the single cell dynamics of CD4+ T cell activation by dendritic cells in lymph nodes. J Exp Med. 2004; 200:847–856. [PubMed: 15466619]

Miller MJ, Wei SH, Cahalan MD, Parker I. Autonomous T cell trafficking examined in vivo with intravital two-photon microscopy. Proc Natl Acad Sci USA. 2003; 100:2604–2609. [PubMed: 12601158]

Miller MJ, Wei SH, Parker I, Cahalan MD. Two-photon imaging of lymphocyte motility and antigen response in intact lymph node. Science. 2002; 296:1869–1873. [PubMed: 12016203]

Monks CR, Freiberg BA, Kupfer H, Sciaky N, Kupfer A. Three dimensional segregation of supramolecular activation clusters in T cells. Nature. 1998; 395:82–86. [PubMed: 9738502]

Pentcheva-Hoang T, Egen JG, Wojnoonski K, Allison JP. B7-1 and B7-2 selectively recruit CTLA-4 and CD28 to the immunological synapse. Immunity. 2004; 21:401–413. [PubMed: 15357951]

Rothlein R, Dustin ML, Marlin SD, Springer TA. A human intercellular adhesion molecule (ICAM-1) distinct from LFA-1. J Immunol. 1986; 137:1270–1274. [PubMed: 3525675]

Rothlein R, Springer TA. The requirement for lymphocyte function-associated antigen 1 in homotypic leukocyte adhesion stimulated by phorbol ester. J Exp Med. 1986; 163:1132–1149. [PubMed: 3517218]

Shakhar G, Lindquist RL, Skokos D, Dudziak D, Huang JH, Nussenzweig MC, Dustin ML. Stable T cell-dendritic cell interactions precede the development of both tolerance and immunity in vivo. Nat Immunol. 2005; 6:707–714. [PubMed: 15924144]

Sims TN, Soos TJ, Xenias HS, Dubin-Thaler B, Hofman JM, Waite JC, Cameron TO, Thomas VK, Varma R, Wiggins CH, et al. Opposing Effects of PKCtheta and WASp on Symmetry Breaking and Relocation of the Immunological Synapse. Cell. 2007; 129:773–785. [PubMed: 17512410]

Stinchcombe JC, Majorovits E, Bossi G, Fuller S, Griffiths GM. Centrosome polarization delivers secretory granules to the immunological synapse. Nature. 2006; 443:462–465. [PubMed: 17006514]

Tang Q, Adams JY, Tooley AJ, Bi M, Fife BT, Serra P, Santamaria P, Locksley RM, Krummel MF, Bluestone JA. Visualizing regulatory T cell control of autoimmune responses in nonobese diabetic mice. Nat Immunol. 2006; 7:83–92. [PubMed: 16311599]

van Kooyk Y, van de Wiel-van Kemenade P, Weder P, Kuijpers TW, Figdor CG. Enhancement of LFA-1-mediated cell adhesion by triggering through CD2 or CD3 on T lymphocytes. Nature. 1989; 342:811–813. [PubMed: 2574829]

Wang X, Rickert M, Garcia KC. Structure of the quaternary complex of interleukin-2 with its alpha, beta, and gammac receptors. Science. 2005; 310:1159–1163. [PubMed: 16293754]

Williams MA, Tyznik AJ, Bevan MJ. Interleukin-2 signals during priming are required for secondary expansion of CD8(+) memory T cells. Nature. 2006; 441:890–893. [PubMed: 16778891]

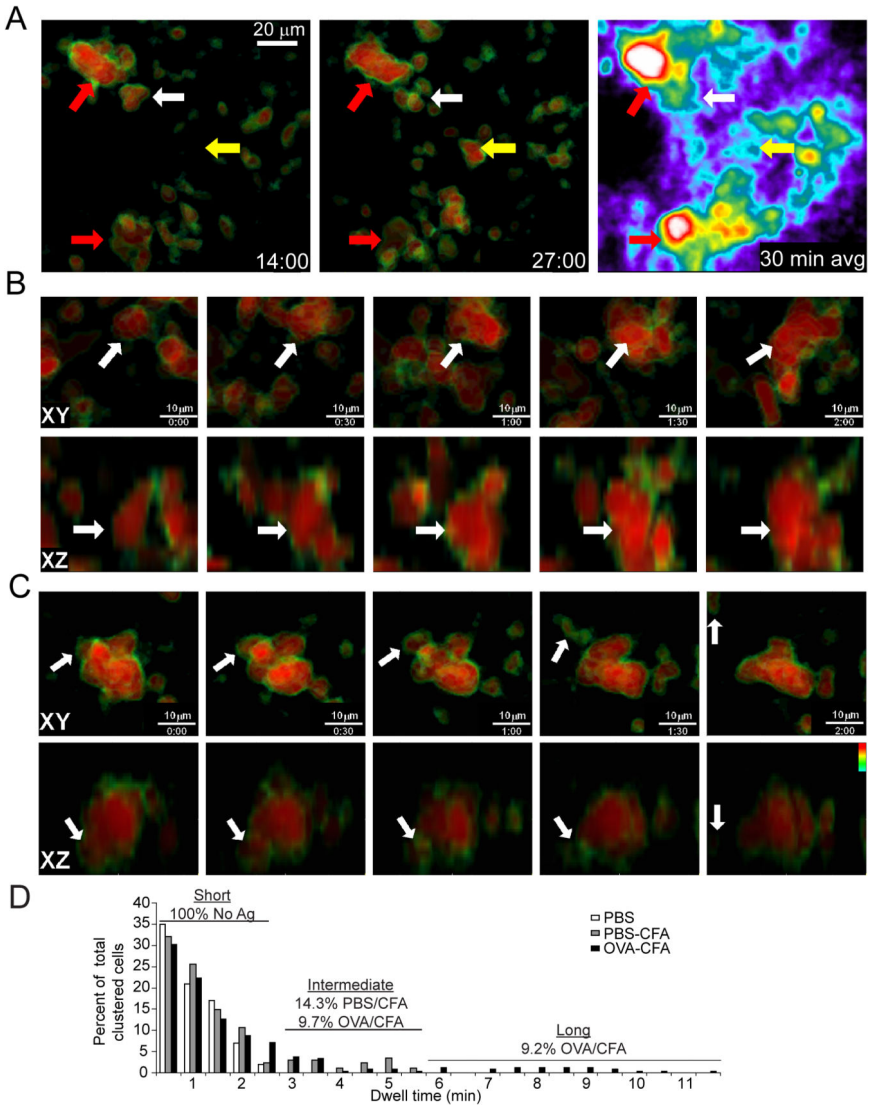

Figure 1. Swarming activation clusters during TCR-dependent T cell activation in vivo

Explant popliteal LN from WT Balb/c mice injected with CFSE-labeled DO11.10 T cells were removed 24h after OVA-CFA immunization and were imaged for 30 minute (min) timelapses. Data are representative of more than five independent experiments. **(A)** Projection images of 312 μm (x) × 260 μm (y) × 150 μm (z) deep data stack. Large 'stable' (red arrows) and small 'transient' (white and yellow arrows) clusters are shown at two timepoints (left two panels) in which CFSE is pseudo-colored (black-green-yellow-red) on a scale that highlights the cell borders as a result of their slightly-reduced fluorescence intensity. The right hand panel is a time-average of an entire 30 min run showing the spatial persistence of cells in the two 'stable' clusters and only weak persistence of cells in the smaller clusters. **(B, C)** Cropped data of two large clusters showing fusion and dispersal. Time stamp, min:sec. **(B)** The fusion of a mid-size cluster (estimated to contain 3-4 cells initially) with other individual and clustered T cells over a 2 min period. Viewing XY and XZ projections of the cluster (indicated by arrow) permits the same cluster to be observed as other clusters and cells join from multiple directions. **(C)** A single T cell leaves a cluster and

crawls away over a 2 min period. Note the appearance of the green-border around the departing cell at min 1, indicative of the movement out of the cluster in XY (top panel) and XZ (lower panel) dimensions. **(D)** Dwell time of transient ‘small’ clusters as a function of immunization condition. Any close T-T contact was scored for the length of interaction prior to dispersal (and represented as a percent of total T-T interactions scored). PBS-only, unimmunized control; OVA-CFA, draining LN; PBS-CFA, control immunized LN. At least 19 couples were scored for each condition.

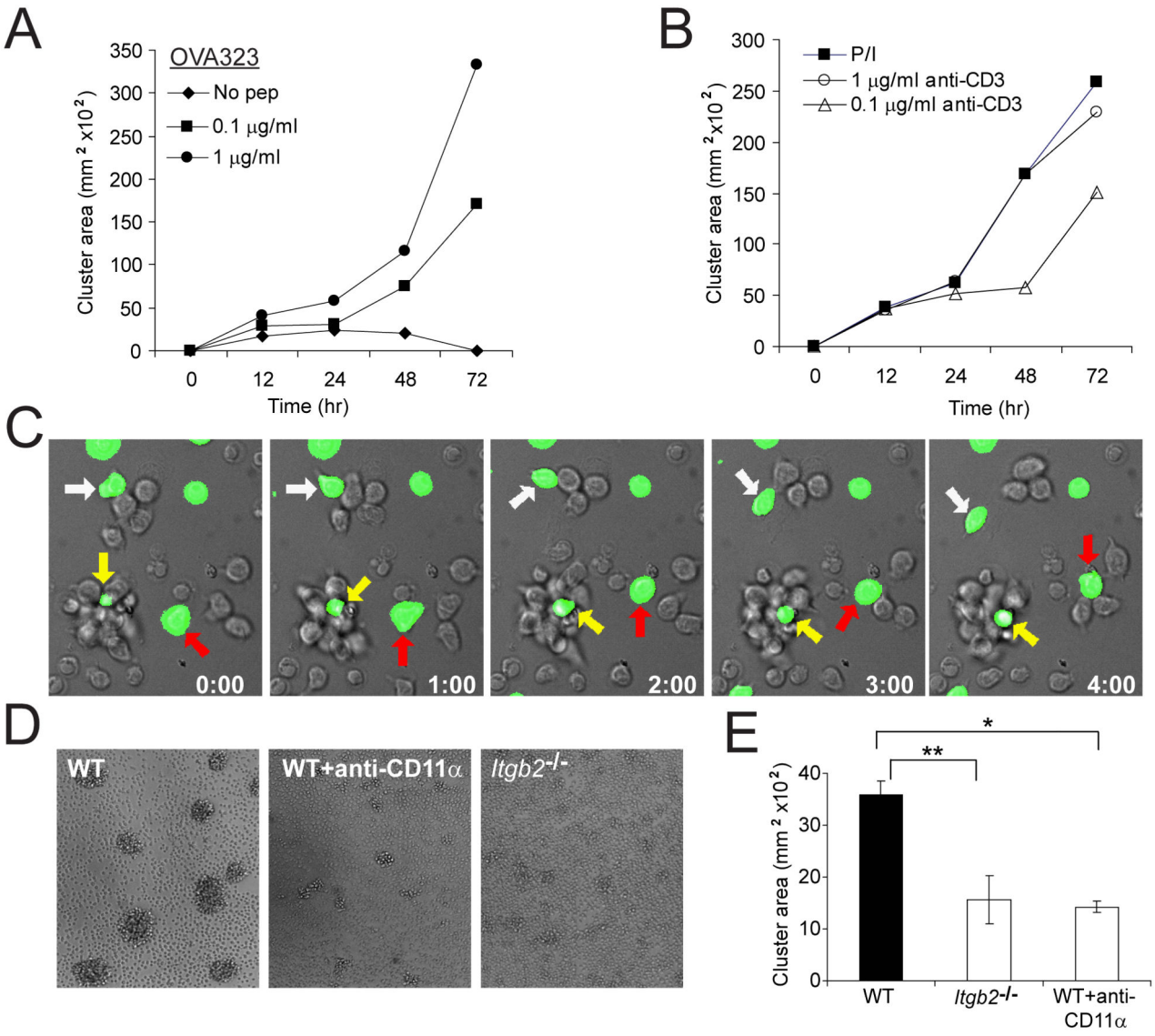

Figure 2. Dynamic activation clusters in vitro utilize LFA-1 to assemble

(A) Whole DO11.10 LN cells were activated in vitro with titrated doses of OVA 323 (0-1 μg/ml); wells were photographed at the indicated timepoints. The cross-sectional (xy) area of clusters is shown as a function of time. Data is representative of two independent experiments. **(B)** DO11.10 $CD4^+$ T cells were activated with PMA and ionomycin, or titrated plate-bound anti-CD3 with soluble anti-CD28 (5 μg/ml); cluster formation over time represented as in **A**. Data is representative of two independent experiments. **(C)** C57BL/6 $CD4^+$ T cells (90% unlabeled, 10% CFSE-labeled) were stimulated with PMA and ionomycin, and time-lapse microscopy was performed 18h after stimulation. Differential interference contrast (DIC) and green fluorescence from CFSE were acquired every 20 sec over 5 min. White arrows indicate a dissociating cell; red arrows indicate a cell joining a cluster; yellow arrows indicate a persistent cluster. Time stamp, min:sec. **(D, E)** B6 WT or LFA-1-deficient *Itgb2*$^{-/-}$$CD4^+$ T cells were stimulated for 20h with PMA and ionomycin. At 18h, some B6 WT cells were treated with anti-CD11α (LFA-1) antibody (20 μg/ml).

Cluster formation was assessed at 20h as above. In **D**, representative pictures of clusters; in **E**, graphical representation of clustering. *, two-sample $t(94)=1.986$, $p=1.14\times10^{-13}$; **, two-sample $t(93)=1.986$, $p=1.75\times10^{-12}$. Data are representative of two to three independent experiments.

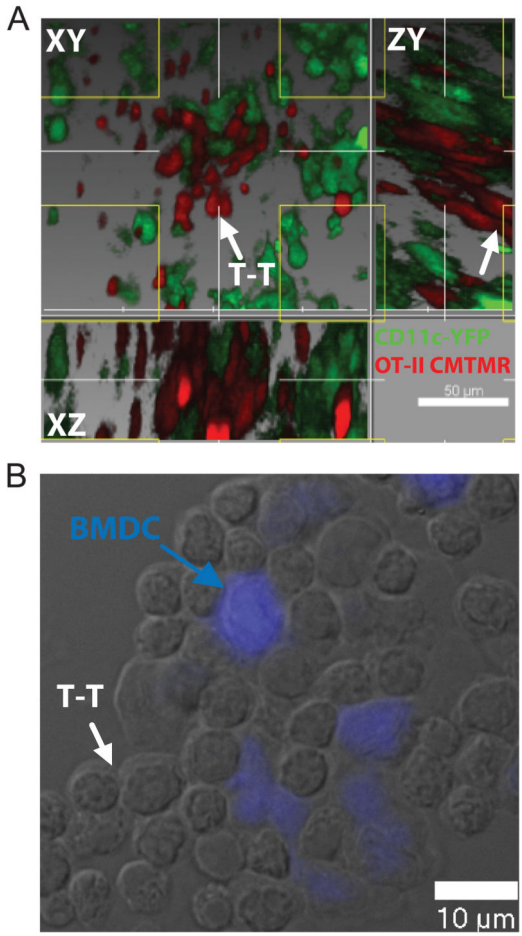

Figure 3. Relationship of T-APC contacts to T-T contacts

(A) CMTMR-labeled OT-II CD4$^+$ T cells were injected into CD11c-YFP mice which were immunized subcutaneously with OVA-CFA, and the draining LN was isolated for TPSLM after 24h, corresponding to phase II of T cell activation. A region containing clusters demonstrates a majority of T cells forming simultaneous contacts with APC and one another and a smaller cohort engaging in homotypic interactions at some distance from the nearest DC. White arrow indicates a T-T contact distal to adjacent DC cell bodies. Note that the T cell zone contains a meshwork of DC and it is highly probable that any T cells will lie within a distance of less than 20 μm from a visible dendritic cell body while within this zone, regardless of their potential interactions. **(B)** OT-II CD4$^+$ T cells were activated in vitro for 20h with C57BL/6 BMDC, pre-labeled with OVA 323 and CMAC (blue). Note that some lateral T-T interactions occur for T cells directly contacting APC whereas additional T cells homotypically interact beyond the evident DC border. Data representative of at least three independent trials.

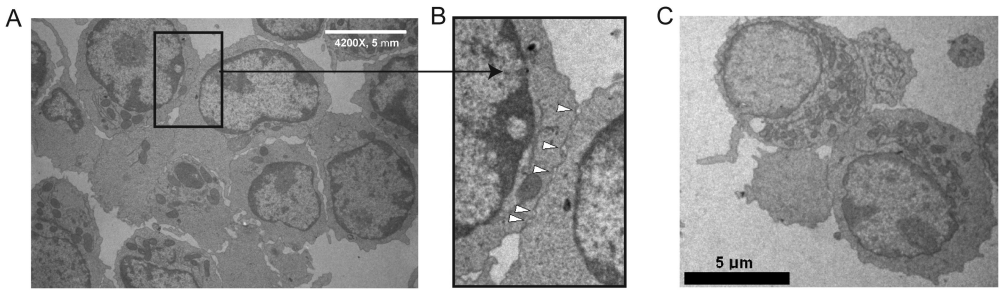

Figure 4. Ultrastructural features of T-T clusters

Balb/c WT $CD4^+$ T cells were stimulated with PMA and ionomycin; 18h after stimulation, EM was performed. **(A)** Representative picture of interacting T cells, with inset showing a T-T interface. **(B)** Magnification of a T-T synaptic region, showing synaptic gaps between tightly-apposed membranes. **(C)** Representing view of cell conjugate showing intracellular vesicles positioned opposite one another in the 2 primary cells.

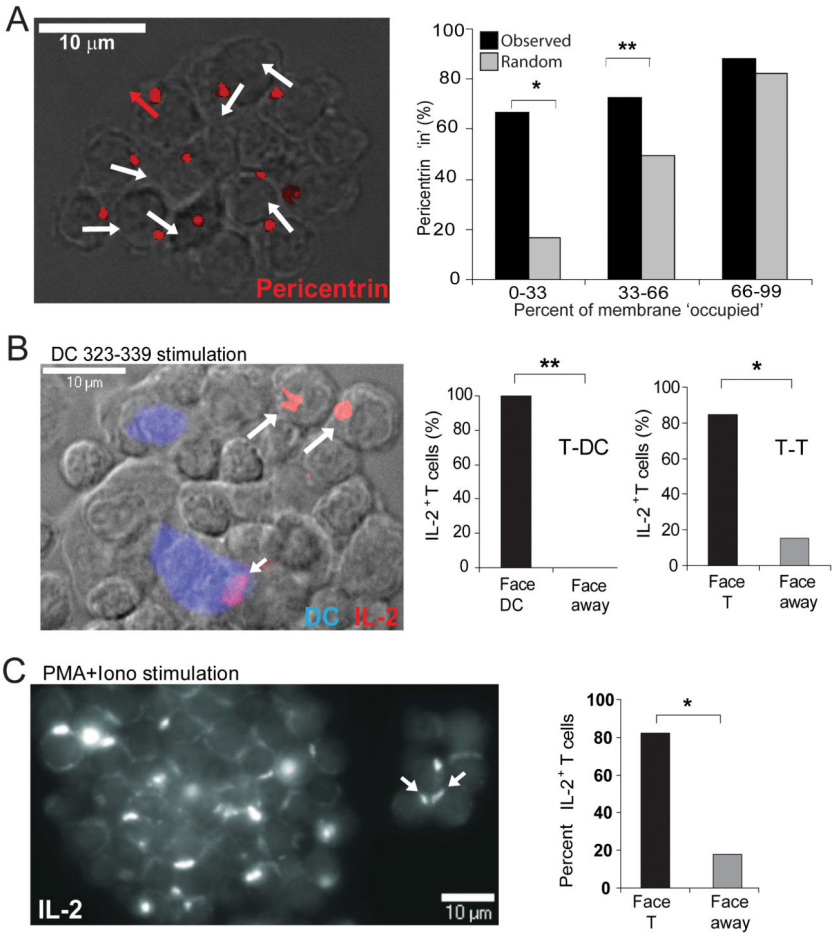

Figure 5. Polarized secretion and receptor aggregates between T cells in clusters

(A) Pericentrin is detected facing inward after activation with PMA and ionomycin. DO11.10 $CD4^+$ T cells were stimulated for 19h with PMA and ionomycin; permeabilized clusters fixed to slides were stained with purified anti-pericentrin Ab. Pericentrin shown in red; white arrows indicate pericentrin stain localized into cluster; red arrows indicate pericentrin pointed outward from T cluster. Graph represents the actual percent of pericentrin 'in' (black bars) versus the predicted percent of pericentrin that would be expected to face 'in' (gray bars) if the polarization were due to the percent of available T-T membrane interface (x-axis). *, P=0.00001, **, P=0.002; determined by Chi-squared goodness of fit test. **(B)** IL-2 is polarized inward toward DC and T contacts in clusters when activated by peptide-pulsed DCs. OT-II $CD4^+$ T cells were activated for 20h with actin-CFP^+ BMDC, pre-pulsed with OVA 323 (10 μg/ml). Permeabilized clusters were stained with anti-IL-2 Ab. DCs in blue on widefield DIC overlay and IL-2 in red. In the graphs, IL-2 localization is represented as the percent of IL-2^+ T cells pointing in toward a facing T cell or pointing away from a neighboring T cell for all IL-2^+ T-T pairs (only border cells scored); and as the percent of IL-2-positive T cells pointing toward a DC, or away from the DC, for all IL-2^+ T-DC pairs. *, P<0.0004, **, P<0.005. **C)** IL-2 is polarized inward toward T-T contacts after PMA and ionomycin stimulation. DO11.10 $CD4^+$ T cells were stimulated as in **A** and stained as in **B**. IL-2 shown on a grey-scale in a z-reconstruction of a large (left)

and small (right) cluster. IL-2 localization is graphically represented as the percent of IL-2^+ T cells pointing in toward a facing T cell (open symbol) or pointing away from a neighboring T cell (closed, red symbol). The average exposed surface was at least 50% for all of these measurements. *, P<0.0001..

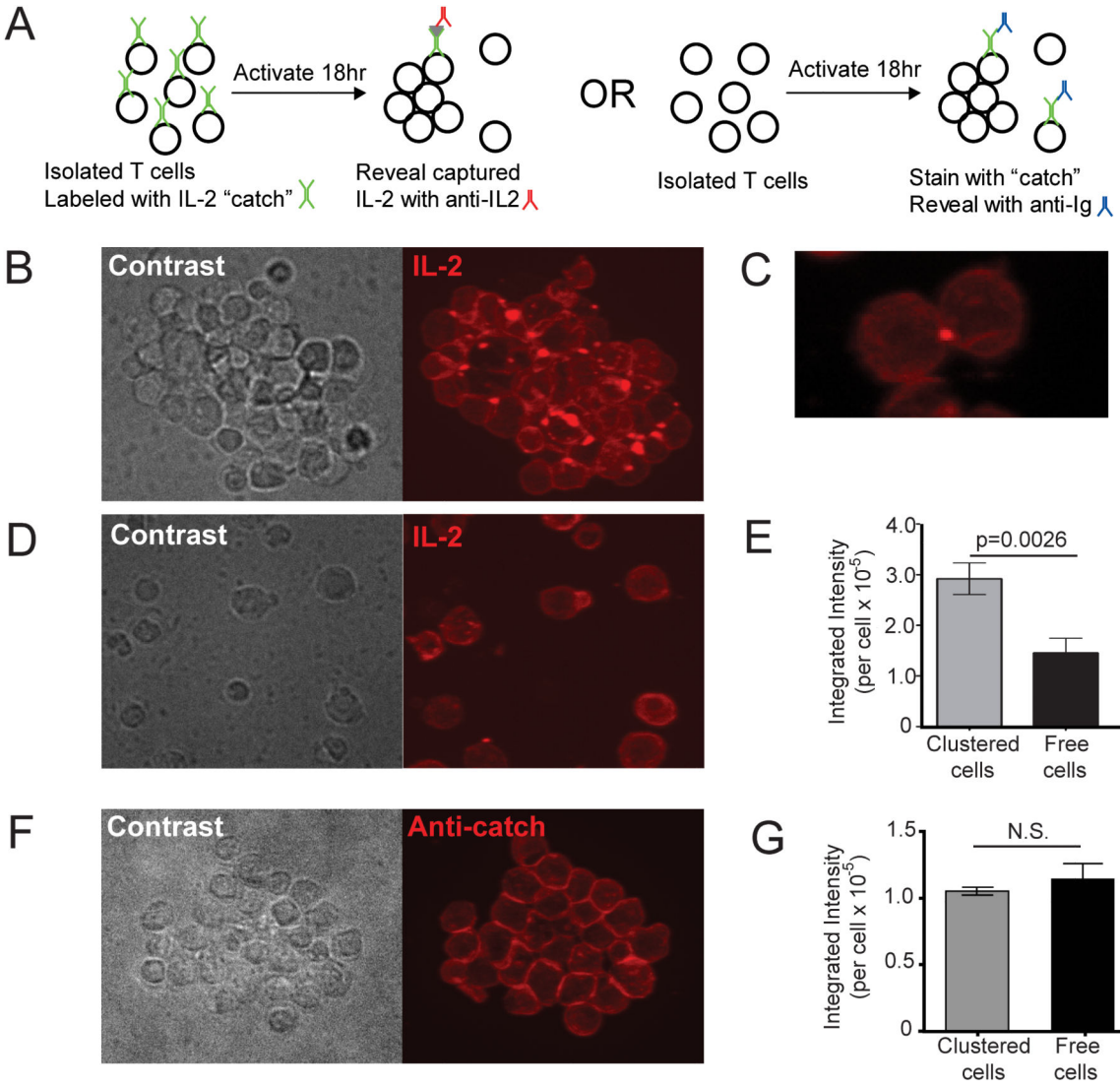

Figure 6. Preferential Capture of IL-2 within synaptic Regions of T-T clusters

(A) Scheme for identifying spatial parameters for IL-2 capture by T cells. **(B-E)** IL-2 catch reagent coated Balb/c WT $CD4^+$ T cells were stimulated with PMA and ionomycin for 19h, fixed with PFA and stained with PE-conjugated IL-2 detection Ab. Representative images of clustered cells **(B, C)** and free cells **(D)**, and mean fluorescence intensity of IL-2 detection antibody staining per cell (**E**, n = 586 for clustered cells and n = 52 for free cells) are depicted. Data are representative of three independent experiments. **(F-G)** Balb/c $CD4^+$ T cells were stimulated with PMA and ionomycin for 19h, fixed with PFA, coated with IL-2 catch reagent, and stained with rhodamine conjugated secondary Ab against catch reagent (anti-catch). Representative image of clustered cell **(F)** and mean fluorescence intensity of secondary antibody staining per cell (**G**, n = 215 for clustered cells and n = 28 for free cells) were depicted. All the fluorescence images are maximum projection of z-stacks.

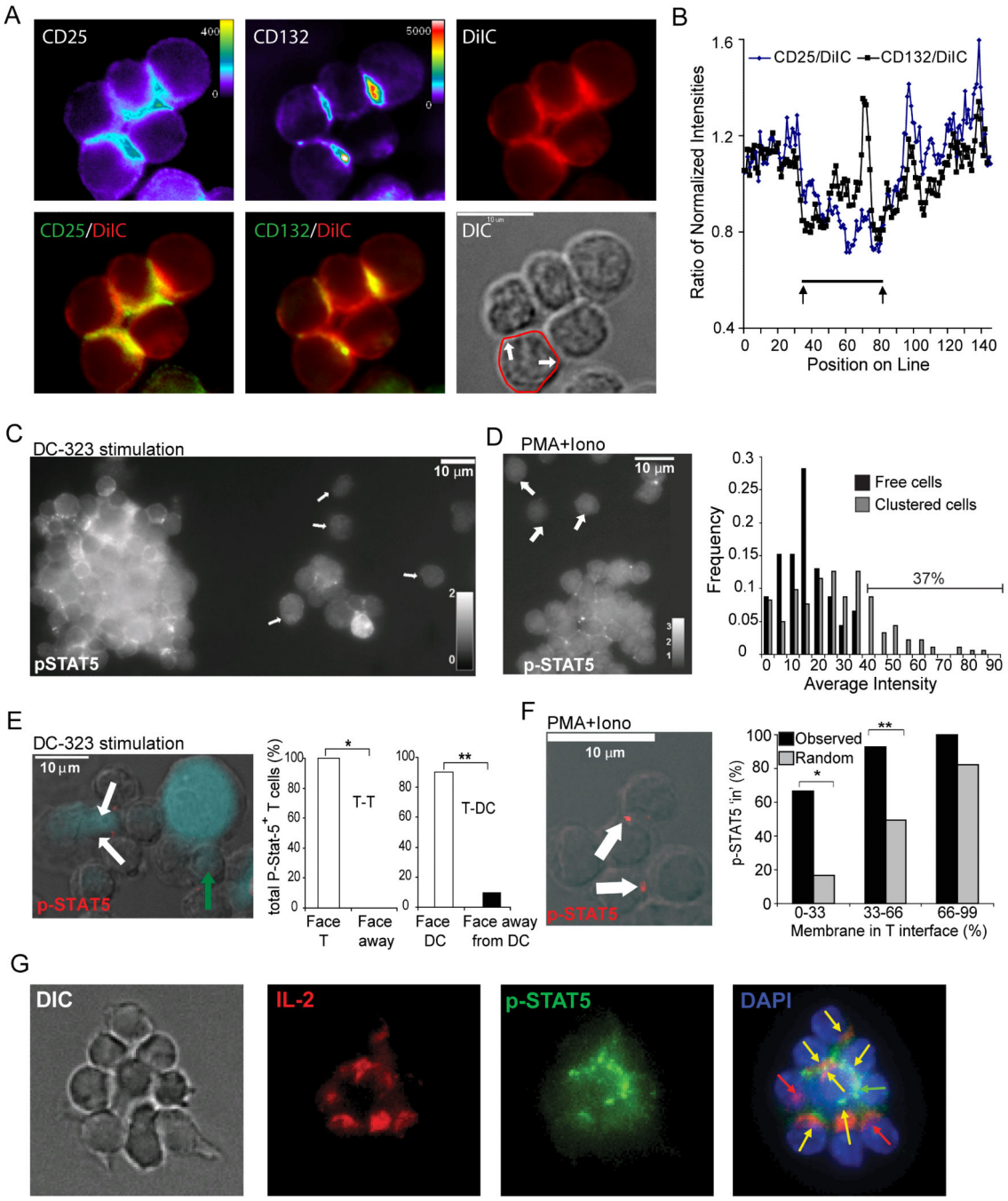

Figure 7. IL2 Receptor Signaling Across T-T Synapses

(A) Purified CD4$^+$ T cells were activated for 19h with PMA and ionomycin, and stained with antibodies to CD25, CD132 and with membrane staining dye DiIC. Overlays of CD25-DiIC and CD132-DiIC are shown in order to accentuate regions at which antibody staining intensity exceeded membrane intensity. **(B)** A linescan (starting from at the back of the contact, shown overlaid onto the DIC image in **A**) of the membrane domain of a single T cell is shown compared for the three stains at the same focal place. Normalized intensities were compared on a pixel-by-pixel basis and demonstrate a peak of CD132 accumulation in

the central contact region (**C, E**) OT-II $CD4^+$ T cells were activated for 20h with actin-CFP^+ BMDC, pre-pulsed with OVA 323 (10 μg/ml). Permeabilized clusters were stained with anti-phospho-STAT5 Ab. In **C**, the image is shown as a three-dimensional maximal-intensity projection, and p-STAT5 stain is represented in white, with arrows indicating free cells. In **E**, DCs are represented in blue on the widefield DIC overlay with p-STA-5 antibody in red; white arrows indicate p-STAT5 localized in toward a DC, green arrow indicates p-STAT5 pointing inward toward a T cell. p-STAT5 localization is graphically represented as the percent of p-$STAT5^+$ T cells pointing in toward a facing T cell (green symbol) or pointing away from a neighboring T cell for all p-$STAT5^+$ T-T pairs; and as the percent of p-$STAT5^+$ T cells pointing toward a DC (open symbol), or away from the DC (closed symbol), for all p-$STAT5^+$ T-DC pairs. *, $P<0.008$, **, $P<0.00001$. **(D, F)** $CD4^+$ T cells were activated for 19h with PMA and ionomycin. Clusters were harvested and stained as above. In **D**, a 3D projection of the entire cell volume is shown and p-STAT-5 stain is represented in white, with arrows indicating free cells. Graph represents the frequency of p-STAT5 fluorescent intensities (with background subtracted) for clustered (grey symbol) and free (black symbol) cells. In **F**, p-STAT5 is red on the widefield DIC overlay; white arrows indicate p-STAT-5 localized in toward a T cell; white bar indicates 10μm. Graph represents the actual percent of p-STAT5 facing 'in' (black bars) versus the predicted percent of p-STAT-5 that would be expected to face 'in' (gray bars) if the polarization were due to the percent of available T-T membrane interface (x-axis). *, $P=0.0192$, **, $P=0.0011$; determined by Chi-squared goodness of fit test. **(G)** $CD4^+$ T cells were stimulated with PMA and ionomycin for 18h and stained for anti-p-STAT5 and anti-IL-2; cells were co-stained with DAPI. Depicted are DIC (left), IL-2 (red, 2nd panel), p-STAT5 (3d panel, green), and an overlay of IL-2 (red), p-STAT-5 (green) and DAPI (blue) (4th panel). Arrows are as follows: green, localization of p-STAT5 only; red, localization of IL-2 only; and yellow, co-localization of p-STAT5 and IL-2. Bars, 10 μm. Data are representative of two independent experiments.